LATERAL INTERACTIONS AMONG MEMBRANE PROTEINS

Valid Estimates Based on Freeze-Fracture Electron Microscopy

JOCHEN BRAUN, JAMES R. ABNEY, AND JOHN C. OWICKI
Department of Biophysics and Medical Physics, University of California, Berkeley, and Division of Biology and Medicine, Lawrence Berkeley Laboratory, University of California, Berkeley, California 94720

ABSTRACT We consider the lateral distribution of intrinsic membrane proteins from the viewpoint of the statistical-mechanical theory of liquids. We connect the information in freeze-fracture electron micrographs—positions of proteins but not lipids or aqueous species—to a well developed theory of liquid mixtures. An algorithm, based on the Born–Green–Yvon integral equation, is presented for deducing forces between proteins from correlations among protein positions that are observed in micrographs. The algorithm is tested on simulated micrographs, obtained by Monte-Carlo methods, where forces between proteins are known analytically. We conclude that valid estimates of such forces, both attractions and repulsions, can be obtained from the positions of a few thousand proteins.

1. INTRODUCTION

Most research on the structure of biological membranes has focused on transmembrane organization, i.e., the location of molecules and functional groups along a line normal to the membrane surface. A smaller body of research, of which this paper is a part, addresses an orthogonal problem: the nature and basis of the lateral distribution of molecules in membranes.

Biological membranes generally are not ideal lateral mixtures of their components. Inhomogeneous lateral distributions of both lipids and proteins are well documented and reflect the functional specialization of different regions of membrane (for reviews see Oliver and Berlin, 1982; Fraser and Poo, 1982; Jain, 1983; Malhotra, 1983; Holmes et al., 1984; Almers and Stirling, 1984; Gumbiner and Louvard, 1985). Striking examples of large-scale ($\sim\mu$m) inhomogeneities in the distribution of intrinsic membrane proteins include the ion channels in myelinated nerve fibers (Waxman and Ritchie, 1985), the purple patches in the membranes of halophile bacteria (Stoeckenius et al., 1979), and the densely packed plaques in gap junctions (Loewenstein, 1981; Peracchia, 1985). Less well studied are smaller-scale (10–100 nm) heterogeneities that may reflect, among other things, enzymatic pathways and recognition mechanisms. The triggering of degranulation by the local clustering of immunoglobulin E receptors in mast cells and basophils is one example of the latter (Metzger and Ishizaka, 1982).

Such phenomena can have diverse causes, including the attachment of proteins to extramembranous structures. In the absence of such factors, the distributions must reflect forces acting within the membrane. Further, it should be possible to obtain information on these forces by using statistical-mechanical methods to analyze the positional correlations among the proteins. Freeze-fracture electron microscopy is a convenient source of data about the lateral distribution of intrinsic membrane proteins. The analysis of forces based on such micrographs began over a decade ago (Markovics et al., 1974) and has been reviewed recently (Abney and Owicki, 1985).

The present paper contains two theoretical and one empirical contributions to the subject. First, it shows how the overall problem can be embedded in a powerful statistical-mechanical approach, essentially the MacMillan–Mayer theory of solutions. This permits a more rigorous treatment, allows a semi-quantitative discussion of approximations, and suggests extensions by connection to an already well-developed body of theory. Second, the paper presents and tests an improved algorithm for obtaining forces from electron micrographs, a method based on the Born–Green–Yvon (BGY) integral equation.

Assuming that electron micrographs accurately represent the positions of particles in an equilibrated fluid, the question remains whether the number of particles that can realistically be observed in a freeze-fracture electron micrograph is sufficiently large, i.e., whether positional

J. Braun's present address is Department of Applied Mathematics and Computer Science, Weizmann Institute for Science, Rehovot, 76100, Israel.

Address correspondence to J. C. Owicki.

correlations can be determined with sufficient precision, for the inference of particle interactions to be meaningful. We address this question empirically: by simulating fluids whose particles interact with known pair potentials, then inferring pair potentials from the positions of a thousand to a few tens of thousands of particles, and finally comparing these computed pair potentials with the fluids' true pair potentials. We conclude that valid estimates for a pair potential can be obtained, in particular if the BGY scheme is used, from the positions of a few thousand particles.

A companion paper (Abney et al., 1987) applies the theoretical results to the structure of gap junctions. A preliminary report of some of this work has appeared elsewhere (Braun et al., 1984).

2. THEORY

In this part of the paper we derive the general relations that allow the extraction of some information about particle interactions from observed particle positions. We follow standard textbook accounts on the statistical mechanics of fluid mixtures, particularly the McMillan–Mayer theory of solutions (e.g., Hill, 1956, 1960; McQuarrie, 1976).

2.1. If Only One Species Is of Interest, a Fluid Mixture Can Be Treated Formally Like a Pure Fluid

Consider an equilibrated fluid composed of an arbitrary number of polyatomic species 1, 2, 3, . . . as an open system characterized by a volume V, a temperature T, and the activities z_1, z_2, . . . of each species. A patch of membrane—containing a protein species, assorted lipid species, water, and other components—is an example of such a fluid. We restrict our attention to a single phase of the system; if two or more phases are present (for example, protein-rich and protein-poor), then the theory can be applied separately within each phase.

Assume that we are interested in species 1 (here, the membrane proteins) and that we have some means of observing the center-of-mass positions of all such molecules. The set of center-of-mass positions of all N_1 molecules of species 1 may be called the configuration of species 1 and denoted $\{N_1\}$. The total configuration of the fluid (i.e., all coordinates of all $\mathbf{N} = N_1, N_2, \ldots$ molecules) is denoted $\{\mathbf{N}\}$. It is useful to separate the degrees of freedom that are of interest to us: $\{\mathbf{N} - N_1\}$ refers to all coordinates other than those in $\{N_1\}$. Besides center-of-mass coordinates of species 2, 3, . . . , $\{\mathbf{N} - N_1\}$ specifies the rotational and conformational coordinates of all species, including species 1.

The conditional probability of encountering a total configuration, $\mathbf{N}$, given that N_1 molecules of species 1 have a configuration $\{N_1\}$, is

$$P(\{\mathbf{N}\}|\{N_1\}) = \frac{z_2^{N_2} z_3^{N_3} \ldots e^{-\beta U(\{N_1\},\{\mathbf{N}-N_1\})}}{\Psi_{N_1} N_2! N_3! \ldots}. \quad (1)$$

Here, β is $1/kT$ (where k is the Boltzmann constant) and $U(\{N_1\}, \{\mathbf{N} - N_1\})$ is the total potential energy of the fluid. Ψ_{N_1} is the partition fluid for a system that contains N_1 molecules of (observed) species 1 and is open with respect to the other species.

We now derive an expression for the effective force exerted on one molecule of species 1 by the remaining molecules of that species. For a given total configuration, $\{\mathbf{N}\}$, the actual force on molecule i of species 1 is simply the negative gradient of the total configuration potential, $-\nabla_i U(\{N_1\}, \{\mathbf{N} - N_1\})$. For a given configuration, $\{N_1\}$, the effective force, $\mathbf{f}_i(\{N_1\})$, can be defined as the average actual force on molecule i of species 1:

$$\mathbf{f}_i(\{N_1\}) \equiv \langle -\nabla_i U(\{N_1\}, \{\mathbf{N} - N_1\}) \rangle_{\{\mathbf{N}-N_1\}}$$
$$= \int -\nabla_i U(\{N_1\}, \{\mathbf{N} - N_1\}) P(\{\mathbf{N}\}|\{N_1\})\, \mathrm{d}\{\mathbf{N} - N_1\}. \quad (2)$$

The average is taken over the entire set of total configurations that are consistent with the configuration $\{N_1\}$, i.e., over all possible $\{\mathbf{N} - N_1\}$. Note that the effective force defined in this way depends on the positions of all molecules of species 1.

Finally, we turn to the effective configuration potential, $U(\{N_1\})$, which we define by integrating over all unobserved degrees of freedom:

$$e^{-\beta U(\{N_1\})} \equiv \frac{\sum_{N_2,N_3,\ldots=0}^{\infty} \frac{z_2^{N_2} z_3^{N_3} \ldots}{N_2! N_3! \ldots} \int e^{-\beta U(\{N_1\},\{\mathbf{N}-N_1\})}\, \mathrm{d}\{\mathbf{N} - N_1\}}{\sum_{N_2,N_3,\ldots=0}^{\infty} \frac{z_2^{N_2} z_3^{N_3} \ldots}{N_2! N_3! \ldots} \int e^{-\beta U(\{0\},\{\mathbf{N}\})}\, \mathrm{d}\{\mathbf{N}\}}. \quad (3)$$

Note that in the denominator the total configuration potential is for a fluid devoid of species 1, i.e., $N_1 = 0$. We also define the associated canonical effective configuration integral

$$Z_{N_1} = \int e^{-\beta U(\{N_1\})}\, \mathrm{d}\{N_1\}. \quad (4)$$

From these definitions follow several properties of $U(\{N_1\})$ that justify its interpretation as an effective configuration potential for species 1: First, $U(\{N_1\})$ is zero if N_1 is zero, i.e., it is associated with the presence of molecules of species 1. Second, its gradient with respect to the position of a molecule of species 1 is the effective force on that molecule. Third, it can be used to form a configuration integral, Z_{N_1}, that governs the probability for encountering a particular configuration, $\{N_1\}$. Fourth, this configuration integral will be seen to be related to osmotic pressure in the way expected of a quantity bearing the name (see Section 2.5).

The three quantities we have defined, configuration probability, effective force, and effective configuration potential, permit us formally to treat a fluid mixture as we would treat a pure fluid. Only the adjective "effective," qualifying force and potential of the fluid, reminds us of the presence of other molecular species. The unobserved

species and the unobserved degrees of freedom of the observed species manifest their effects only through the functional form of $U(\{N_1\})$. For example, the effects of deviations from cylindrical symmetry in a membrane protein are integrated in a Boltzmann-averaged sense (Eq. 3) and are replaced by effective cylindrically symmetric interactions. Henceforth all the forces and potentials that we discuss will be implicitly effective ones; we will simplify notation by usually omitting the species subscript from N_1, $\{N_1\}$, $U(\{N_1\})$, etc., and will from now on refer to "particles" rather than molecules of species

In a fluid of N (observable) particles, the conditional probability density, $\rho^{(n)}(n)$, of encountering any n particles in the partial configuration $\{n\}$, regardless of the positions of the remaining $N - n$ particles, is

$$\rho^{(n)}(\{n\}) = \frac{N!}{(N-n)!}\int \frac{e^{-\beta U(\{N\})}}{Z_N}\, d\{N-n\} \equiv \rho^n g^{(n)}(\{n\}). \quad (5)$$

Here, the braces $\{N - n\}$ denote all possible configurations of the $N - n$ particles whose positions are not specified by $\{n\}$. The second equation defines the n-body correlation function, $g^{(n)}(\{n\})$, where ρ stands for the number density of (observable) particles. If the particles do not interact, i.e., if their positions are not correlated, then the left-hand side of the equation simply equals ρ^n and the correlation function, $g^{(n)}$, equals one identically.

In a homogeneous isotropic fluid the pair ($n = 2$) correlation function for particles at $\mathbf{r}_1$ and $\mathbf{r}_2$, is termed the radial distribution function, written simply as $g(r_{12})$. Under similar conditions, the triplet correlation function is written $g^{(3)}(r_{12}, r_{13}, r_{23})$.

2.2. The Assumption of Pair-Wise Additivity and Three Schemes for Estimating a Pair Potential or Force

Further progress is difficult without assuming that the effective configuration potential, $U(\mathbf{r}_1, \ldots, \mathbf{r}_N)$, is a sum of pair potentials, $u(r_{ij})$, which depend on the pair separation r_{ij} and, in general, on the state of the fluid as well:

$$U(\{N\}) = \sum_{i>j} u(r_{ij}). \quad (6)$$

This has been called the assumption of "pair-wise additivity." Though a good approximation for simple liquids, its validity for interacting membrane proteins is less clear. Our treatment proceeds on the basis of this assumption to obtain a tentative pair potential, which can then be submitted to a kind of self-consistency test that may vindicate the assumption of pair-wise additivity in retrospect (see Sections 2.3 and 5.3).

With this assumption, the defining equation for correlation functions becomes

$$\rho^n g^{(n)}(\{n\}) = \frac{N!}{(N-n)!}\frac{\int e^{-\beta\sum_{i>j} u(r_{ij})}\, d\{N-n\}}{Z_N}. \quad (7)$$

The problem now at hand is to invert this integral equation to obtain the pair potential, $u(r_{ij})$, as a function of some correlation function, $g^{(n)}(\mathbf{r}_1, \ldots, \mathbf{r}_n)$. This so-called "inverse problem" has a long history in the physics of fluids and we limit ourselves to describing three inversion schemes.

(*a*) *Scheme 1.* Obtaining a pair potential from the observed radial distribution function and angle-integrated triplet distribution function as the solution of the Born–Green–Yvon equation.

The radial distribution function can be used to define a quantity, $u_M(r_{12})$, through

$$u_M(r_{12}) \equiv kT \ln [g(r_{12})]. \quad (8)$$

As a consequence of this definition and Eq. 5,

$$f_M(r_{12}) \equiv -\nabla_1 u_M(r_{12}) = \frac{\int (-\nabla_1 U(\{N\}))e^{-\beta U(\{N\})}\, d\{N-(1,2)\}}{\int e^{-\beta U(\{N\})}\, d\{N-(1,2)\}}. \quad (9)$$

In other words, $-\nabla_1 u_M(r_{12})$ is the mean force exerted on particle 1 along the line $\mathbf{r}_{12}$ by the $N - 1$ other particles while particle 2 occupies position $\mathbf{r}_{12}$. For this reason, $f_M(r_{12})$ is called the mean force and $u_M(r_{12})$ the potential of mean force. These quantities are useful because they represent a reference point for understanding particle–particle interactions, albeit without distinguishing between direct interactions of particles 1 and 2 and the indirect interactions involving all the other particles. That distinction can be made explicit with the assumption of pair-wise additivity:

$$f_M(r_{12}) = -\frac{\nabla_1 g(r_{12})}{\beta g(r_{12})} = -\nabla_1 u(r_{13}) + \int (-\nabla_1 u(r_{13}))\frac{g^{(3)}(r_{12}, r_{13}, r_{23})}{g^{(2)}(r_{12})}\, d\mathbf{r}_{13}. \quad (10)$$

This is the Born–Green–Yvon equation, an integral equation in the pair potential, $u(r_{ij})$, the radial distribution function, $g(r_{12})$, and the triplet distribution function $g^{(3)}(r_{12}, r_{13}, r_{23})$. It identifies the contributions to the mean force on particle 1 as, first, the force exerted by particle 2 and, second, the forces exerted by other particles at all positions of the plane. Given particles at $\mathbf{r}_1$ and $\mathbf{r}_2$, the

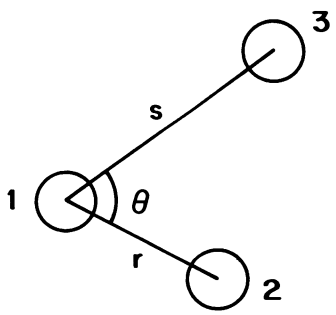

FIGURE 1 The polar coordinate system used in the BGY formalism, Eqs. 11 and 12.

average number density of other particles at any $\mathbf{r}_3$ is $\rho g^{(3)}(r_{12}, r_{13}, r_{23})/g(r_{12})$. For a pair-wise additive fluid, Eq. 10 is exact. Note that, as $\rho \to 0, f_M(r) \to -\nabla u(r)$.

For our purposes, the BGY equation can be rewritten in planar polar coordinates (Fig. 1):

$$\frac{g'(r)}{\beta g(r)} = u'(r) + \int_0^\infty u'(s)K(r, s)\,ds, \tag{11}$$

where prime denotes differentiation with respect to argument and $K(r, s)$ is defined as

$$K(r, s) \equiv \int_0^{2\pi} \frac{\rho g^{(3)}(r, s, \vartheta)}{g(r)} \cos(\vartheta) s\,d\vartheta. \tag{12}$$

If the radial distribution function, $g(r)$, and the angle-integrated triplet distribution function, $K(r, s)$, are known, this linear integral equation can be solved directly for the pair force, $f(r) = -u'(r)$. The pair force can then be integrated to yield a pair potential, $u(r)$.

The BGY equation is fundamental to the theory of fluids, but our application of it to the inverse problem is, we believe, novel. Our method is based on the availability of both pair and triplet distribution functions for membrane proteins. Only pair distribution functions can be determined for more familiar three-dimensional fluids (by diffraction methods); components of these systems cannot in general be imaged by methods comparable to freeze-fracture electron microscopy.

(*b*) *Scheme 2.* Numerical simulation of particles interacting with pair potentials that are adjusted iteratively until the computed radial distribution function matches the one observed in a real fluid.

Using Monte-Carlo or molecular-dynamics techniques for simulating a system of N particles interacting with a pair potential, a set of particle positions can be generated from which correlation functions such as the radial distribution function can be determined. Depending on the deviation of this simulated distribution function from the radial distribution function observed in a real fluid, the pair potential can be modified and the procedure repeated until the two distribution functions match. On the order of a dozen iterations are sufficient, since one can predict roughly how the pair potential must be changed to bring the two distribution functions into closer agreement (Levesque et al., 1985).

This procedure shares with Scheme 1 the advantage of yielding a pair potential, that is, in principle at least, as accurate as the observed radial distribution function. However, the computational expense of this procedure is considerable. It was devised for fluids in which only the radial distribution function is known (from scattering experiments) and has been applied to a Lennard–Jones fluid and on a model potential for aluminum (Levesque et al., 1985). For fluids where the particle coordinates themselves are available (such as assemblies of membrane proteins) and where, in consequence, higher order distribution functions can be observed, Scheme 1 is more direct and, we believe more convenient.

(*c*) *Scheme 3.* Deduction of a pair potential from the radial distribution function and the Percus–Yevick approximation.

From the definition of the radial distribution function, $g(r_{12})$, it is clear that $g(r_{12}) - 1$ is a measure of the total "influence" of particle 1 on particles at $\mathbf{r}_2$. This total influence, $h(r_{12}) \equiv g(r_{12}) - 1$, can be thought divided into a direct and an indirect part. The direct part is given by a "direct correlation function," $c(r_{12})$, and the indirect part is the influence of particle 1 on third particles that is propagated further to particles at $\mathbf{r}_2$. This decomposition of $h(r_{12})$ is expressed by the Ornstein–Zernicke equation:

$$h(r_{12}) \equiv c(r_{12}) + \rho \int c(r_{13})h(r_{23})\,d\mathbf{r}_3. \tag{13}$$

Using Fourier transforms, this equation can be solved analytically for $c(r)$. Between the direct correlation function, $c(r)$, and a pair potential, $u(r)$, there exists an approximate relation, namely the Percus–Yevick (PY) closure:

$$c(r) = e^{-\beta u_M(r)} - e^{-\beta[u_M(r) - u(r)]} = g(r)(1 - e^{\beta u(r)}). \tag{14}$$

This relation approximates $c(r)$ as the total correlation between particles 1 and 2, minus that part of the correlation that is not due to the pair potential $u(r)$. A more complete rationale for this approximation can be found in McQuarrie (1976). Together, Eqs. 13 and 14 provide an analytic, if approximate, expression for a pair potential, $u(r)$, in terms of the radial distribution function, $g(r)$.

The PY approximation should give good results when the range of strong interactions is much shorter than typical distances between neighboring particles, $\sim\rho^{-1/2}$. The results will deteriorate at higher densities; accuracy is sacrificed for computational simplicity. The PY equation is only the best known of many approximate integral equations that can be applied to the inverse problem (McQuarrie, 1976; Levesque et al., 1985); others might prove useful for analyzing membrane proteins but have not yet been applied in this context.

2.3. Pair Potentials: Computed, Apparent, and True

Some circumspection is necessary in interpreting a pair potential obtained through one of the schemes described in Section 2.2. All three are computed pair potentials that are the products of algorithms that assume pair-wise additivity. If that assumption is valid under the conditions for which the fluid was analyzed, then we say the computed pair potentials are also apparent pair potentials and that the fluid is apparently pair-wise additive. Pair potentials obtained by the BGY and simulation methods (Schemes 1 and 2) will then be identical, and the PY potential will differ from them only to the extent of the density-dependent error in the PY approximation.

A stronger requirement is that the assumption of pair-wise additivity hold over all conditions, for example, all densities. If it does, then the computed pair potentials are not only apparent, but true pair potentials, and the fluid is truly pair-wise additive. The same pair potential governs the interactions of two isolated particles and two particles in the bulk of the liquid at nonzero density. The pair potentials from the three schemes have the same relationships as described in the previous paragraph.

Fluids can be apparently, but not truly, pair-wise additive. For example, at high densities, long-range multibody interactions felt by isolated particles may become hidden; their contribution to the effective configuration potential may become independent of the particular configuration and come to depend on density alone (Pearson et al., 1984).

If the assumption of pair-wise additivity is violated, then in general the computed pair potentials from the three schemes will differ from one another. Each will reach a different compromise in incorporating some average of the higher-body potentials. Moreover, correlation functions generated from the computed potentials by numerical simulation methods will in general differ from correlation functions in the real fluids. Specifically, the BGY potential will reproduce neither the pair nor the triplet correlation function; the simulation potential, which must succeed on the pair correlation function, will fail on the triplet function. These observations can be used to detect the presence of multibody terms in the configuration potential (see Section 5.3).

2.4. The Pressure Equation

The pair potential of a pure and pair-wise additive fluid determines not only microscopic properties of the fluid, such as correlation functions, but macroscopic properties, such as the pressure or the free energy, as well. In a fluid mixture, the effective pair potential of an observable species determines the osmotic pressure, i.e., the pressure difference one would observe between the mixture and a fluid containing all species except the observable one. In the case of a biological membrane, the osmotic pressure is the pressure difference between a patch of membrane containing proteins and adjacent regions devoid of protein. Since this quantity is of biological interest, we briefly describe how the osmotic pressure can be calculated from an effective pair potential and the radial distribution function.

In an open system, the pressure is conveniently determined from the grand-canonical partition function. In a system that is closed with respect to species 1 but open to all other species, the pressure is determined from the semi-grand-canonical partition function Ψ_{N_1}.

$$p = kT\left(\frac{\partial \ln \Psi_{N_1}}{\partial V}\right)_{T,z}. \tag{15}$$

The osmotic pressure between a fluid containing N_1 molecules of species 1 and a fluid devoid of species 1 (e.g., the pressure across a partition impermeable to species 1 but permeable to all species other than species 1) is

$$\frac{\Pi(N_1)}{kT} = \left(\frac{\partial \ln Z_{N_1}}{\partial V}\right)_{T,z}. \tag{16}$$

From this one may derive the so-called pressure equation which, for a two-dimensional pair-wise additive fluid, reads

$$\frac{\Pi}{kT} = \rho + \frac{\rho^2}{4kT}\int_0^\infty rf(r)g(r)2\pi r\,dr. \tag{17}$$

3. METHODS

3.1. Simulation of Fluids with Purely Repulsive and with Attractive Intermolecular Forces

The choice of simulation potentials was motivated by the desire to analyze our technique with a force similar to that expected for protein–protein interactions in experimental systems. This stipulated the choice of softer repulsions than those found in the hard-core or Lennard–Jones potentials that are commonly used in simulations of simple liquids. In dense simple fluids, attractions do not affect structural features much, even though they may be important thermodynamically (Widom, 1967). Therefore, we also wanted to test the ability of the technique to detect relatively weak attractions.

We report results for simulations based on the 6-4 pair potential, defined as

$$u_{6\text{-}4}(r) \equiv \frac{27}{4}\epsilon[(\sigma/r)^6 - (\sigma/r)^4]. \tag{18}$$

The potential crosses zero at $r = \sigma$; ϵ is the depth of the potential well at its minimum, attained at $r = r_0 = (3/2)^{1/2}\sigma$ (see Fig. 2). The 6-4 pair force is found by differentiation.

$$f_{6\text{-}4}(r) = -u'_{6\text{-}4}(r) = 27\epsilon\,[(\sigma/r)^5 - 3/2(\sigma/r)^7]. \tag{19}$$

This force is repulsive for $r < r_0$ and attractive for $r > r_0$.

A fluid with attractions (fluid A) was simulated with essentially the 6-4 potential. However, for computational economy the potential was truncated at $r = 2.5r_0 = 3.0619\sigma$ and shifted up slightly (by $u_{6\text{-}4}(2.5r_0) \approx 0.07\epsilon$) to maintain continuity, so that the actual potential used was

$$u_A(r) = \begin{cases} u_{6\text{-}4}(r) - u_{6\text{-}4}(2.5r_0) & r < 2.5r_0 \\ 0 & r \geq 2.5r_0. \end{cases} \tag{20}$$

This truncation leaves the force unaltered, except that $f_{6\text{-}4}(r) = 0$ for $r \geq 2.5r_0$.

A purely repulsive fluid (fluid R) was simulated with a potential created by subtracting from the 6-4 potential its minimum value, $u_{6\text{-}4}(r_0) = -\epsilon$, and setting the potential

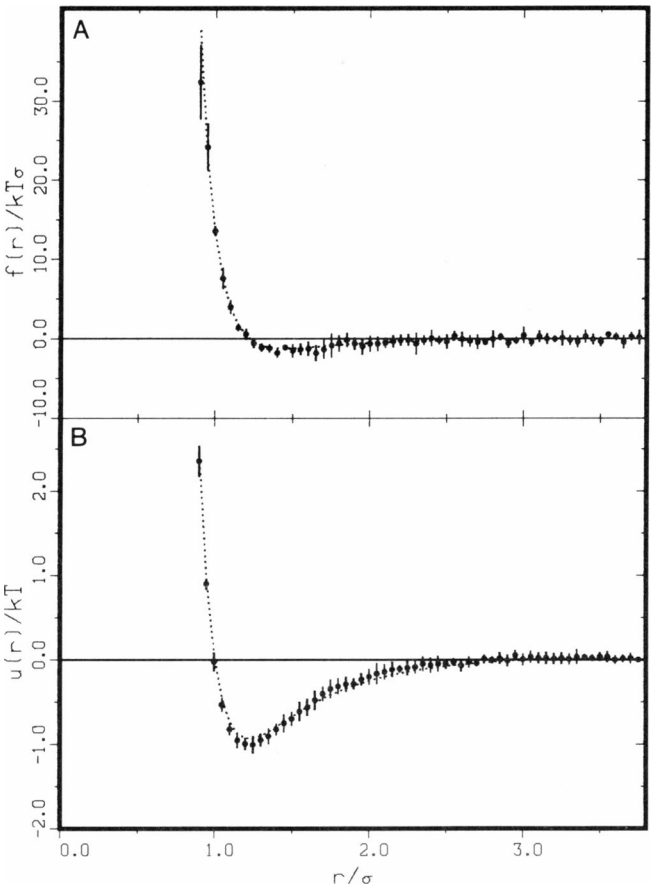

FIGURE 2 Pair force $f_A(r)$ (A) and pair potential $u_A(r)$ (B) for the attractive fluid A: analytical functions and results of BGY analysis. Smooth dotted lines are the analytical functions from Eqs. 20 and 19 (the latter truncated at $r = 2.5r_0$). Large dots respresent the combined BGY analysis of six 4,096-particle patches. Vertical error lines are the standard errors of these estimates. The bin width Δ for the BGY analysis was 0.075σ.

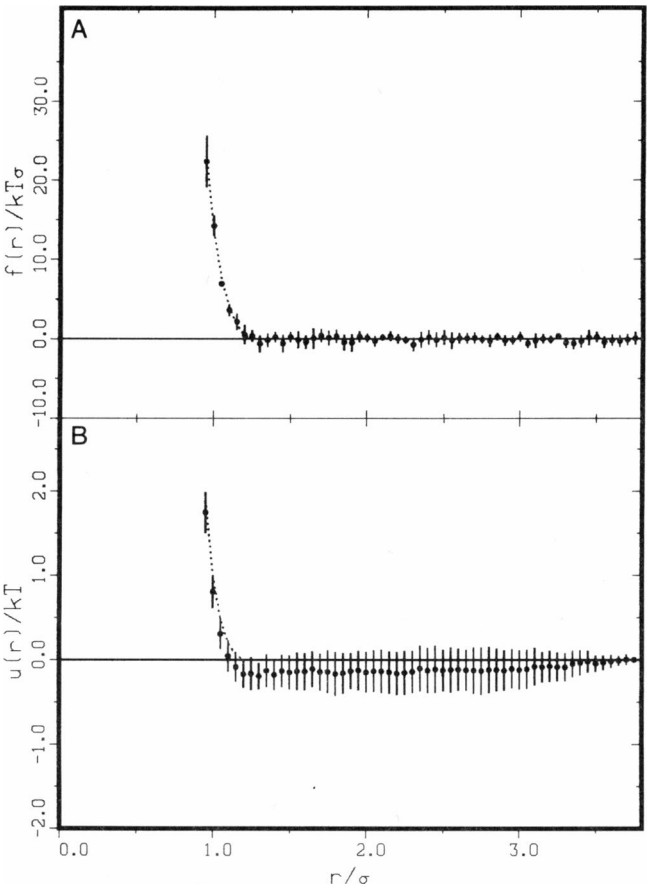

FIGURE 3 Pair force $f_R(r)$ (A) and pair potential $u_R(r)$ (B) for the purely repulsive fluid R: analytical functions and results of BGY analysis. Analytical functions are taken from Eqs. 21 and 19 (the latter truncated at $r = r_0$). Figure organization is the same as that of Fig. 2.

equal to zero beyond $r = r_0$:

$$u_R(r) = \begin{cases} u_{6\text{-}4}(r) - u_{6\text{-}4}(r_0) & r < r_0 \\ 0 & r \geq r_0 \end{cases} \quad (21)$$

See Fig. 3. This is the Weeks-Chandler-Andersen decomposition, which preserves precisely the repulsive component of the 6-4 potential (Chandler et al., 1983). The force is zero in the attractive domain of the 6-4 potential, i.e., for $r \geq r_0$.

To generate samples of coordinates for particles interacting with these potentials we used the standard Metropolis et al. (1953) Monte-Carlo algorithm. We simulated 256, 1,024, or 4,096 particles in square domains (patches). To avoid special treatment of particles close to the boundary of the domain, we used permeable boundaries and periodic boundary conditions. In this way, we approximated a square domain within the bulk of the fluid. The results of simulations of this type are considered indistinguishable from observations on a physical system interacting with the chosen potential. We simulated liquids R and A at reduced temperature $T^* \equiv \epsilon/k = 1.0$, rendering the depth of the well in $u_A(r) \sim 1\ kT$, and at reduced number density $\rho^* \equiv \rho\sigma^2 = 0.5$, rendering the characteristic particle separation $\rho^{-1/2} = 2^{1/2}\sigma = (4/3)^{1/2}r_0$.

The choice of these values for T^* and ρ^* ensured that (a) the system's attractive well in $u(r)$ was thermally significant but not overpowering, and (b) the chosen density and potential very qualitatively reproduced the situation observed for gap junction particles in mouse liver (see companion paper by Abney et al. [1987]).

Simulations were begun by equilibrating a crystalline array of 256 particles for (typically) 1,000 to 5,000 stochastic steps per particle. This economically generated a representative sample of the fluid but contained too few particles for our purposes. To form a larger patch we then used four contiguous duplicates of this configuration to form the starting configuration for a patch of 1,024 particles, which we equilibrated with another 100 stochastic steps per particle. This was sufficient to move each particle more than the average particle separation and assured statistical independence of the four quadrants of

the configuration. To obtain a configuration for a patch of 4,096 particles, we repeated this procedure.

3.2. Estimation of Correlation Functions from Patch Configurations

Estimates of two correlation functions, $g(r)$ and $K(r, s)$, must be obtained from each patch analyzed. Such estimates are in principle a straightforward undertaking for which a recipe is provided by the definition of the desired correlation function. In practice, there are two complications. First, the large number of triplets formed from $O(10^3)$ particles necessitates an efficient counting algorithm. The second arises from the need for special treatment of boundary regions. The boundary of a patch, whether taken from a simulation or electron micrograph, is, in general, a convex polygon. Our programs for estimating correlation functions were designed to handle boundaries of this type and could be applied equally well to patches of membrane and simulated fluid.

Because of the finite number of points available, it was necessary to divide particle separations into "bins" of nonzero width Δ, typically 0.05 to 0.10 of the mean separation between neighboring particles. Our results are histograms representing estimates of averages over the bin widths. Thus, for $(n_r - \frac{1}{2})\Delta \le r < (n_r + \frac{1}{2})\Delta$, with $n_r = 1, 2, 3, \ldots,$

$$g(r) \approx \langle g(n_r\Delta)\rangle_{n_r} \equiv \frac{\int_{(n\cdot r-1/2)\Delta}^{(n\cdot r+1/2)\Delta} g(r)2\pi r\,\mathrm{d}r}{2\pi n_r\Delta^2}. \quad (22)$$

The quantity $\langle K(r, s)\rangle_{n_r}$ is defined similarly. Details of the numerical methods for counting triplets efficiently and handling convex polygonal borders of patches correctly are available from the authors.

3.3. Estimation of Pair Forces and Potentials from Correlation Functions

3.3.1. Born–Green–Yvon Scheme. The BGY equation, Eq. 11, is prepared for numerical solution by averaging all terms over annuli in r and displaying the integral over s as a sum of integrals over annuli:

$$\left\langle \frac{\mathrm{d}}{\mathrm{d}r}\ln(g(n_r\Delta))\right\rangle_{n_r} = -\langle \beta f(n_r\Delta)\rangle_{n_r} - \sum_{n_s=1}^{\infty}\int_{(n_s-1/2)\Delta}^{(n_s+1/2)\Delta}\beta f(s')\langle K(n_r\Delta, s')\rangle_{n_r}\,\mathrm{d}s'. \quad (23)$$

Relying on small variations of the functions over the width of an annulus, we make the following approximations:

$$\left\langle \frac{\mathrm{d}}{\mathrm{d}r}\ln(g(n_r\Delta))\right\rangle_{n_r} \sim \frac{\mathrm{d}}{\mathrm{d}r}\ln(\langle g(n_r\Delta)\rangle_{n_r}) \quad (24)$$

$$f(s) \sim \langle f(n_s\Delta)\rangle_{n_s} \quad \text{for} \quad (n_s - \tfrac{1}{2})\Delta < s \le (n_s + \tfrac{1}{2})\Delta. \quad (25)$$

The derivative on the right-hand side of Eq. 24 is to be interpreted in terms of finite differences. We truncate the infinite sum above at $n_s = n_{r,\max}$ and below at $n_s = n_{r,\min}$. Contributions to the equation at large separations are negligible due to the finite range of physical forces. Contributions at very small separations, with $n_{r,\min}$ corresponding to physical overlap of the particles, are small because of the small size of the correlation functions.

These approximations allow us to rewrite the BGY equation as

$$\frac{\mathrm{d}}{\mathrm{d}r}\ln(\langle g(n_r\Delta)\rangle_{n_r} = -\langle \beta f(n_r\Delta)\rangle_{n_r} - \sum_{n_s=n_{r,\min}}^{n_{r,\max}}\langle \beta f(n_s\Delta)\rangle_{n_s}\int_{(n_s-1/2)\Delta}^{(n_s+1/2)\Delta}\langle K(n_r\Delta, s')\rangle_{n_r}\,\mathrm{d}s'. \quad (26)$$

This is a system of inhomogeneous linear independent equations for the average force with matrix components given by the terms involving K and the constant vector given by the terms involving g. Both of the latter are computed directly from the patches, from data correspond to n_r, $n_s = n_{r,\min}, n_{r,\min} + 1, \ldots, n_{r,\max}$.

The derivative in Eq. 26 was taken numerically by a five-point Savitzky–Golay (Savitzky and Golay, 1964) algorithm. The computed force was integrated numerically by Simpson's rule (Bevington, 1969) to give the pair potential.

3.3.2. Percus–Yevick Scheme. In computing a pair force and pair potential through the PY scheme, we followed the example of Pearson and colleagues (1984) and used a variant of a three-dimensional algorithm presented by Lado (1967). Briefly, $h(r)$ ($\equiv g(r) - 1$) is Hankel-transformed to give $h(q)$. From $h(q)$ the Hankel transform, $c(q)$, of the direct correlation function is formed as $c(q) = h(q)/(\rho + h(q))$, which function is then back-transformed to yield $c(r)$ itself. From $c(r)$, the pair potential is obtained with the aid of the PY closure relation, Eq. 14. Averaging over bins is used, as in the BGY case. The pair force can then be found by differentiation.

3.3.3. Mean Force and Potential of Mean Force. The mean force, $f_M(r)$, and potential, $u_M(r)$, can be obtained directly from the pair distribution function with the help of their defining relations, Eq. 8 and its derivative. Again, averaging over bins was employed.

4. RESULTS

4.1. Sample Configurations and Correlation Functions from Simulated Fluids

We simulated six patches of 4,096 particles of fluid R and six patches of 4,096 particles of fluid A, each patch representing a small, square domain of particles in the fluid bulk. Sample configurations are shown in Fig. 4. We treated the positions of particles in simulated fluids exactly as we would treat the positions of membrane proteins obtained from freeze-fracture electron micrographs.

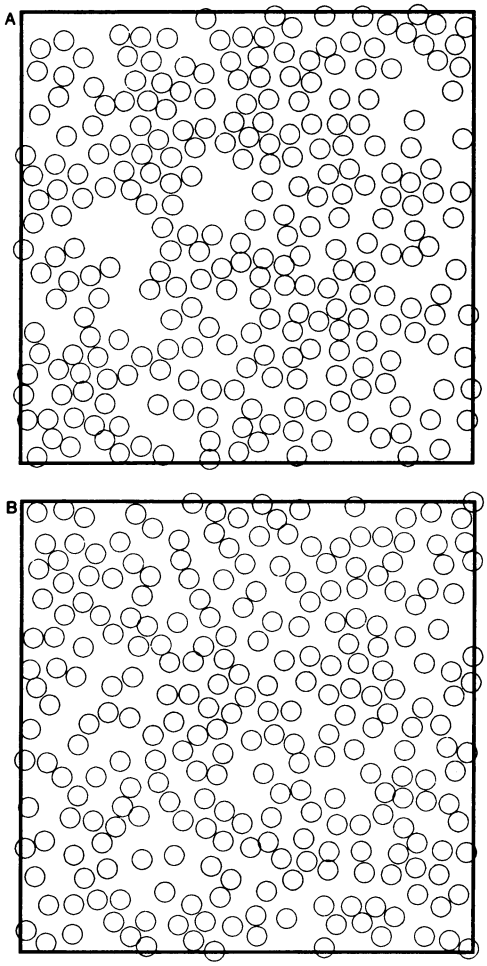

FIGURE 4 Representative configurations from the Monte-Carlo simulations of the attractive fluid A (*A*) and purely repulsive fluid R (*B*). Circle diameters are σ, and only parts of the 4,096-particle configurations are shown. Note that the attractions in the first panel are manifest as a slight tendency toward "patchiness."

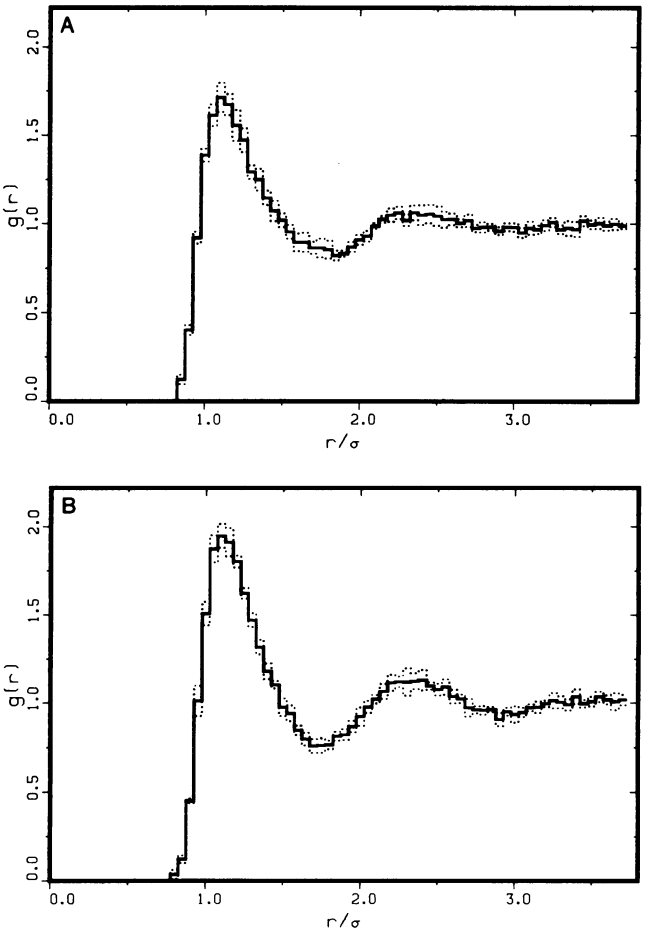

FIGURE 5 Radial distribution functions computed for the attractive fluid A (*A*) and purely repulsive fluid R (*B*). Estimates are based on six 4,096-particle patches for each fluid. The envelopes are the standard errors of the estimates. The two fluids exhibit quite similar pair correlations. The radial distribution function describes the influence of a particle's presence on the neighboring fluid. It measures, relative to the overall particle density, the average particle density on a circle of radius r around a particle whose presence is assumed (the central particle). For dense fluids, the average particle density is zero on circles with small r, since the volume of the central particle excludes other particles from this domain. On successively larger circles, however, the average particle density alternates between values above and below the overall density for a few times. The maxima and minima correspond to a series of concentric rings around the central particle which are, on the average, alternately over- and underpopulated with particles. On even larger circles, the central particle's influence is no longer felt and there the average particle density equals the overall density.

Our computed estimates of the radial distribution functions for the two fluids, $g_A(r)$ and $g_R(r)$, are shown in Fig. 5. The standard errors of the estimates are generally 2 to 5%. The shapes of the distribution functions are typical of those for dense fluids. Note that $g_A(r)$ and $g_R(r)$ are quite similar, despite the presence of attractions in fluid A that are absent in fluid R. This conforms to the discussion in Section 3.1. To recover the correct potentials—purely repulsive vs. repulsive plus attractive—from such structural data alone is a stringent test of a method for solving the inverse problem.

4.2. Pair Forces and Potentials Obtained through the Born–Green–Yvon Scheme

For each of the six fluid patches for fluid A we obtained a pair force through the BGY scheme from its angle-integrated triplet correlation function together with its radial distribution function as described. The average of these determinations is shown in Fig. 2 *A;* integration of these results to give the pair potential $u_{A,BGY}(r)$ is shown in Fig. 2 *B*. The corresponding results for fluid R are given in Fig. 3.

Pair forces and potentials obtained through the BGY scheme agree with the actual pair forces and potentials for both fluids, within the standard errors of the computed quantities as shown by the error bars in the figures. The presence of attractions in fluid A, and their absence in fluid R, is quite clearly shown. This demonstrates that our programs are currently written and that the method does

not suffer from any severe numerical instabilities. Since we know that the fluids are truly pair-wise additive, self-consistency checks on correlation functions (see Section 2.3) are not necessary.

The remaining question is, how many particles need be analyzed to get useful information on forces and potentials? Certainly $N \sim 2.5 \cdot 10^4$, as in Figs. 2 and 3, is adequate for most purposes except, perhaps, the fine details of the poorly sampled highly repulsive region at particle contact. Error bars in the figures scale as $N^{-1/2}$, so features of the potentials $\sim 1kT$ in size are resolvable from the positions of a few thousand particles. Some sample determinations of potentials from patches of 1,024 particles, drawn from the 4,096-particle patches, are shown in Fig. 6. These still indicate the grosser features of the potentials. In most freeze-fracture electron microscopy studies it should be possible to observe several thousand particles, in a series of micrographs if not all in one patch. The computational method should not usually fail for lack of data.

4.3. Pair Potentials Obtained through the Percus–Yevick Scheme

The results of applying the PY scheme to the two simulated fluids are shown in Fig. 7. The potentials of mean force are also shown for reference. The PY analysis overestimates the position and depth of the attractive well for fluid A. For fluid R it exhibits an artifactual hump for $r/\sigma \sim 2$ and great imprecision at close range. Presumably the PY method would have performed better at lower densities, but under these conditions it is clearly inferior to the BGY scheme.

4.4. Miscellaneous Other Results Concerning the Born–Green–Yvon Scheme

We also used our simulations of patches of fluids R and A to investigate a number of technical issues related to the BGY scheme. In summary, we found that (*a*) the pair force is insensitive to the precise "bin width" (width of the sampling annuli) used for establishing radial distribution functions and angle-integrated triplet correlation functions, (*b*) the pair force is insensitive to the precise truncation (largest annulus sampled) used while establishing these functions and, (*c*) that the force obtained as the average of pair forces, which in turn are obtained from correlation functions of individual patches, does not differ significantly from the pair force obtained from correlation functions that in turn are obtained as the average of correlation functions of individual patches.

Sometimes there is a preponderance of negative over positive errors in the calculated small forces in the bins at long range. Upon integration to get the potential, these errors can add up to produce a shallow well of doubtful statistical significance (see Fig. 3, for example). This

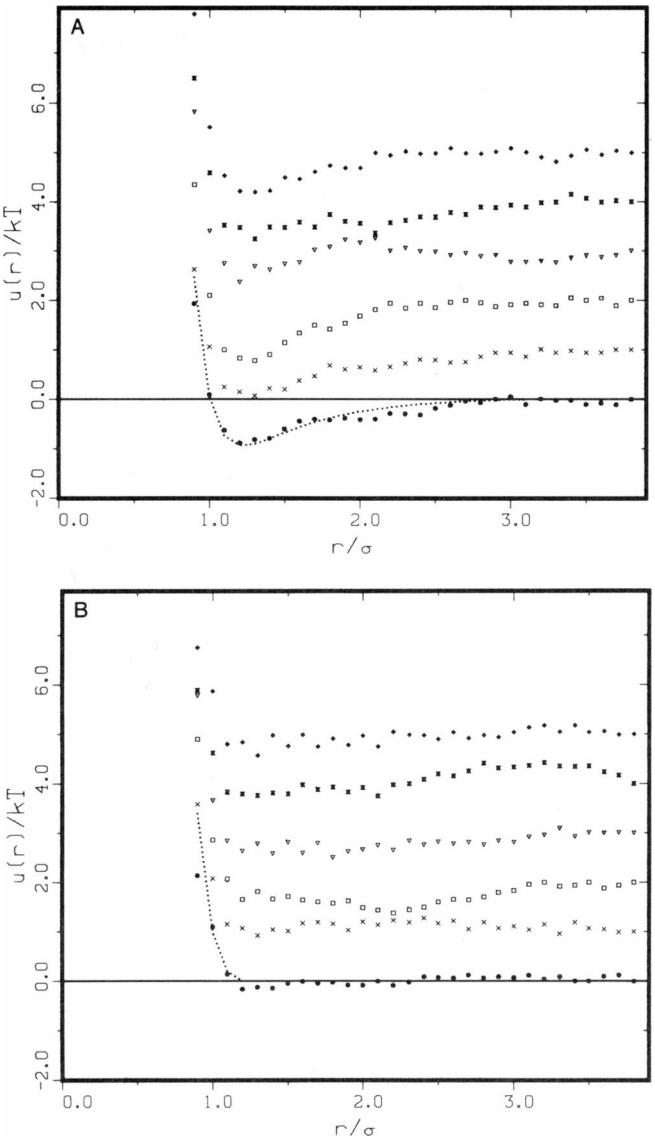

FIGURE 6 Representative pair potentials computed from 1,024-particle configurations by the BGY method for the attractive fluid A (*A*) and purely repulsive fluid R (*B*). The analytical potentials are shown as dotted lines. Results from different configurations are offset vertically for clarity of presentation.

effect, if real, must be a minor artifact of our numerical procedures.

In the absence of triplet configurational data, the triplet correlation function is frequently approximated as a superposition of three pair correlation functions (McQuarrie, 1976):

$$g^{(3)}(r_{12}, r_{13}, r_{23}) \sim g(r_{12})g(r_{13})g(r_{23}). \quad (27)$$

We tested the effects of substituting this for the true triplet data in computing $K(r, s)$ for the BGY analysis. The results were far inferior, closely resembling the mean forces and potentials of mean force.

Finally, we established the satisfactory performance of

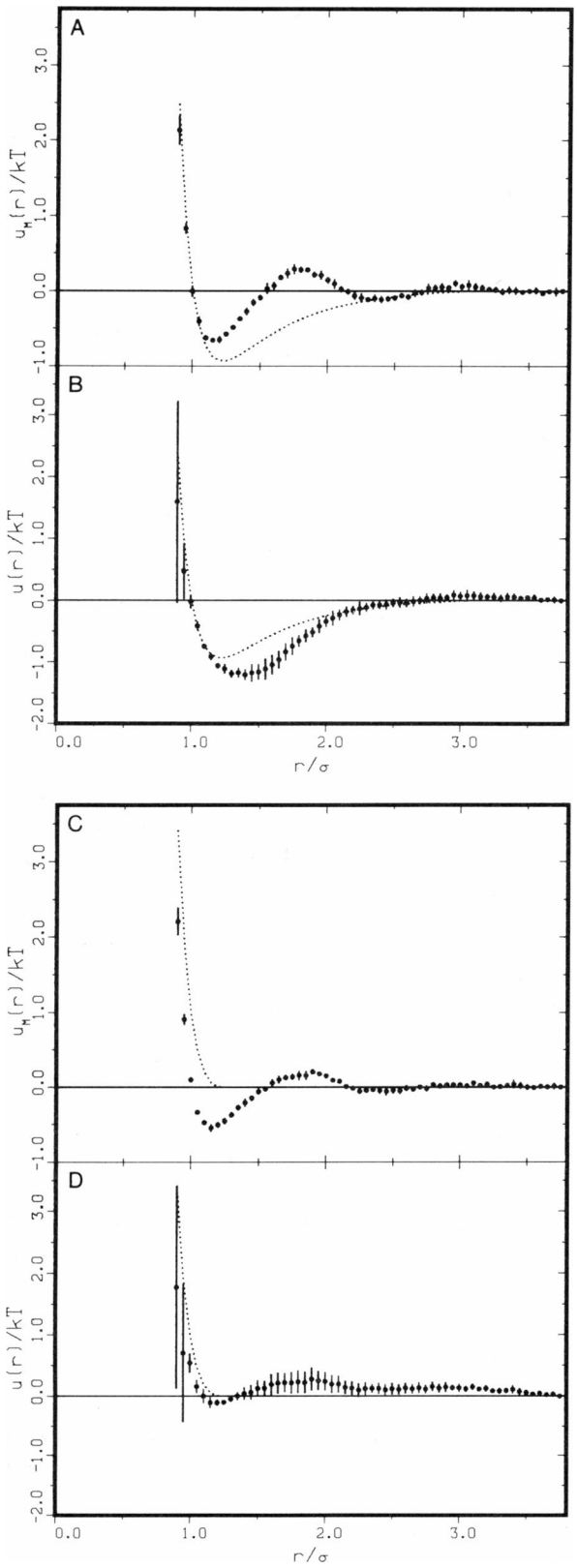

FIGURE 7 Potential of mean force u_M and Percus–Yevick potential determined for the attractive fluid A (*A* and *B*) and the purely repulsive fluid R (*C* and *D*). The dotted lines are the analytical potentials (Eqs. 20 or 21), and standard errors for the computed results are indicated. Computed potentials are from six patches of 4,096 particles for each fluid.

the BGY scheme not only for the "softly" repulsive potentials $u_R(r)$ and $u_A(r)$, but also for several temperatures and densities within the liquid domain of the Lennard–Jones 12-6 potential and for a hard disk system (results not shown).

5. DISCUSSION

5.1. Physical Mechanisms for Lateral Interactions Among Membrane Proteins

Before discussing the theoretical and empirical results presented above, it may prove helpful to list some conceivable physical mechanisms for lateral interactions among membrane proteins. The following list is not intended to be comprehensive.

The first interaction to consider is volume exclusion. It simply reflects the fact that the relative rigidity of proteins must prevent them from approaching each other too closely.

A second is electrostatic. Since identical proteins bear identical charges, the long-range interaction will be repulsive. Shorter-range interactions could be attractive or repulsive, but one would expect repulsions to dominate the averaging that leads to a central-force description. All electrostatic interactions will be screened by counterions to the extent that the aqueous phase and the head groups of charged lipids intervene between the interacting proteins.

Third, stereospecific short-range attractions may occur; a dimerization equilibrium is one example. Although possibly pair-wise additive when described at the level of interacting chemical groups, such additivity is destroyed when the system is analyzed in terms of orientationally averaged central forces.

A fourth, more general, type of protein–protein interaction is indirect, the net effect of degrees of freedom that have been integrated out to achieve the protein-based central-force description of the system. One such interaction involves the perturbation of the conformation of bilayer lipids by the membrane proteins. The details need not concern us here; we merely note that this mechanism may provide an interaction among proteins, probably but not necessarily attractive, which is not pair-wise additive (reviewed by Abney and Owicki, 1985).

If the effective configuration potential of a fluid of membrane proteins is dominated by volume exclusion and electrostatic repulsion, the fluid will be (approximately) truly pair-wise additive. Even if lipid-mediated attractions are significant, however, membrane proteins at sufficiently high densities may still form an apparently pair-wise additive fluid. If the density is decreased to the point where interparticle separations are somewhat beyond the range of the potential, such a fluid will become non–pair-wise additive. Of course, extremely dilute systems are again apparently pair-wise additive, since only pair-wise encounters contribute significantly to the partition function.

5.2. The Validity of Estimates for Protein Interactions Based on Freeze-Fracture Electron Micrographs

The overriding aim of this paper is to convince the readership that estimates based on freeze fracture electron micrographs for lateral interactions among membrane proteins can be valid, i.e., "valid" in the sense of corresponding quantitatively to the forces resulting from physical mechanisms such as those described above.

Generally, an attempt to infer protein interactions is warranted for membranes that are in a state of fluid equilibrium, and that to a very good approximation contain only one species of membrane protein. Excepting extramembranous attachments and two-dimensional protein crystals, membranes resemble very closely an equilibrated two-dimensional fluid (Singer and Nicolson, 1972; McCloskey and Poo, 1984). Equilibration on a short time scale follows from random-walk considerations. These dictate that, for a patch of membrane 0.1–1 μm in diameter, the time required for diffusive equilibration is on the order of seconds; active processes such as the insertion or removal of membrane components, which would tend to disrupt equilibrium, typically occur on a time scale of hours, although receptor recycling can be as fast as $\approx$10 min (Brown et al., 1983). The purity of a membrane's protein component can usually be assessed by biochemical means. A corollary to the requirement for purity is that there must be a fixed number of proteins per particle (preferably one). For a membrane that satisfies these general conditions, the validity of an estimate for protein interactions will turn on three claims, which we will now examine one by one.

(*a*) *Claim 1.* Under experimentally realizable conditions, a freeze-fracture electron micrograph can faithfully represent the essential aspects of the in vivo lateral distribution of membrane proteins.

We judge that freezing rates of 10^6 Ks^{-1} can be attained in the superficial few micrometers of sample using the slamming method of Heuser et al. (1979), and rates above 10^4 Ks^{-1} deeper in the sample or by other freezing methods (see Escaig [1982], Kopstad and Elgsaeter [1982], and Bald [1985]).

By combining simple random-walk statistics with cooling rates and estimated temperature drops required for immobilization, we estimate that proteins diffuse <40 nm when the cooling rate averages 10^4 Ks^{-1} and <4 nm when the rate is 10^6 Ks^{-1} (unpublished results). No large-scale reorganization of the configuration is possible, but redistributions on the scale of nearest neighbors in a dense patch can occur. If the intermolecular interactions are not strongly temperature dependent during the cooling process, the redistribution will not affect the distribution functions beyond the sharpening of features that is characteristic of low-temperature equilibrated fluids. Approximately correct f/kT of u/kT will be computed, though the appropriate T will be below the initial sample temperature.

(*b*) *Claim 2.* A rigorous theory exists for inferring apparent pair forces from observed particle positions.

In Sections 2.1 and 2.2 we outlined a general theory for recovering from observed particle positions functions which we termed "computed pair potentials." If the assumption of pair-wise additivity holds, this theory is rigorous and an apparent pair potential equals a physically meaningful apparent pair potential.

Fortunately, an empirical criterion exists for classifying a fluid pair-wise additive (either "truly" or "apparently") or not. This criterion, essentially a self-consistency test for the assumption of pair-wise additivity, is described further below, in Section 5.3

If, by virtue of passing this test, a fluid is apparently pair-wise additive, then the computed pair potentials obtained through the BGY and the Monte-Carlo scheme equal the apparent pair potential as defined in Section 2.3. Considering accuracy, precision, and convenience, we believe that the BGY technique is the method of choice for analyzing protein interactions from electron micrographs.

Recall that the apparent pair potential may depend on density as well as on particle separation. This apparent pair potential is the potential that would be measured for a pair of particles in the bulk of the fluid. If a fluid can be observed at more than one density, and if the apparent pair potentials at different densities are identical, the fluid is likely to be truly pair-wise additive. In this case, the apparent pair potential is simply the potential that would be measured for an isolated pair of particles. In both cases the apparent pair potential will reflect the physical mechanisms that underlie the effective configuration potential.

If a fluid is non–pair-wise additive, computed pair potentials are more difficult to interpret. In this case pair interactions depend on the position of more than two particles. Computed pair potentials, as functions of only two particle positions, will represent some average of this higher-order function.

(*c*) *Claim 3.* The positions of a few thousand particles suffice for computing a pair potential with acceptable precision.

To support this claim we simulated patches of fluids whose particles interacted with a weakly attractive and/or softly repulsive pair potential. These potentials were qualitatively those expected to obtain between membrane proteins. A potential retrieved from a patch containing a few thousand particles was precise to within $\approx kT$ for particle separations of interest. This was sufficient to reveal weak attractions when these were present, their absence when they were not, and to give an excellent estimate for repulsions. For many membranes it seems likely that rather more particles can be observed and that a correspondingly higher precision can be obtained if necessary. The number of particles required for a given precision will vary inversely with particle density, all else being equal. At

low densities most of the particle separations that are used to form correlation functions are larger than the range of the potential, and the correlations themselves tend to be weaker.

On the strength of the considerations outlined above we think it possible that, for some membranes at least, the factors discussed under all three claims will be favorable and estimated protein interactions will be valid. Of course, ultimately, this question of validity will turn on whether estimates for protein interactions based on observed protein positions will correspond to estimates for protein interactions based on independently determined molecular properties of the proteins and membranes in question.

5.3 A Self-Consistency Test for the Assumption of Pair-Wise Additivity

Conceptually, the test for pair-wise additivity described below rests on the fact that the observed angle-integrated triplet correlation function, a function of two variables, overdetermines the apparent pair potential, a function of one variable, and that, if the observed angle-integrated triplet correlation function does not result from a true pair interaction, a contradiction will result.

Once an apparent pair potential has been obtained through the BGY scheme, the test consists of simulating a patch of a fluid of particles interacting with this apparent pair potential and of determining the radial distribution function in the patch. In other words, the test inverts the inference of "potential from correlation function" and determines whether a computed pair potential would actually result in a fluid with the observed radial distribution function. If radial distribution functions in the simulated patch and the real fluid are identical, the fluid is probably apparently pair-wise additive and possibly even truly pair-wise additive. If they differ, the fluid is non–pair-wise additive. The test can be extended to higher correlation functions.

5.4 Lateral Osmotic Pressure and Large-Scale Heterogeneity in Lateral Distribution

Sometimes a membrane is partitioned into distinct particle-rich and particle-poor regions. One example is gap junctions, which are analyzed in the companion paper (Abney et al., 1987). Such behavior might simply be lateral phase separation under the influence of attractions that can be determined by computing the pair potential in the particle-rich region. Alternatively, the separation might be maintained by other factors, such as barriers to diffusion that originate outside the membrane and are not visible in the micrograph.

Computation of the lateral osmotic pressure, Eq. 17, can differentiate between these cases. This pressure should be essentially zero if the computed pair force governs the large-scale distribution of proteins. A nonzero pressure indicates that additional factors contribute to maintaining the protein density in the populated region. Sometimes computation of the pressure is not necessary for a qualitative result; for example, proteins cannot aggregate solely under the influence of forces that are everywhere repulsive.

5.5 Previous Statistical–Mechanical Analyses of Membrane–Protein Distributions

We consider here only those investigations of the distribution of particles in micrographs that have sought to connect the distributions to intermolecular potentials and forces. Most assaults on the problem have been in the spirit of Scheme 2 (fitting $g(r)$ using numerical simulation), but more approximate. Functional forms for the potentials were assumed, and the fitting consisted of adjusting one or two parameters (e.g., range and strength). The $g(r)$ corresponding to the trial potential was generated by approximate integral equations or by simpler theories applicable to low-density gases.

For example, Markovics et al. (1974) used model potentials and the PY approximation to analyze interactions among pores in nuclear membranes. L. T. Pearson and colleagues used a similar procedure to study bacteriorhodopsin and rhodospin reconstituted into artificial bilayers (Pearson et al., 1983) and cell membranes of *Acholeplasma laidlawii* (Pearson et al., 1984).

Middlehurst and Parker (1986) have considered the effects of deviation from circular (cylindrical) protein shape on $g(r)$. They analyzed hard-core pair potentials without soft repulsions or attractions, e.g., hard rectangles and ellipses. The most striking effect found was a broadening of the initial rise of $g(r)$ from zero at close range, a rise that is discontinuous for hard disks. This is an example of the effects of integrating over unseen degrees of freedom, in this case protein rotation about an axis normal to the bilayer (see Section 2.1). By using Monte-Carlo simulation and hard-ellipse potentials they fit satisfactorily $g(r)$ from erythrocytes (data of R. P. Pearson et al., 1979) and from a barley mutant. Circularly symmetric soft-core interactions can, of course, produce similar effects.

5.6 Previous Application of the Born–Green–Yvon Scheme

We have applied the BGY scheme to gap junction membrane to mouse liver and have obtained an apparent pair potential for the proteins in this membrane (Braun et al., 1984; Abney et al., 1987). We have availed ourselves of the test described in Section 5.3 and have found that the lateral interactions among gap junction proteins are apparently pair-wise additive. This allowed us to interpret the apparent pair potential that we had obtained as the apparent pair potential of gap junction particles at a density of $\approx 10^4$ μm^{-2}. This apparent pair potential explains the observed

radial distribution function and angle-integrated triplet correlation function, as well as the lateral osmotic pressure, which we derived by independent theoretical means. The apparent pair potential we obtained is consistent with electrostatic repulsion and volume exclusion.

We are pleased to acknowledge useful discussions with Karl Runge, Michael Saxton, and Bethe Scalettar. Bethe Scalettar also provided invaluable comments on the manuscript.

This work was supported in part by National Institutes of Health (NIH) grants AI19605 and AI22860 and by a grant form the U. C. Cancer Research Coordinating Committee. J. Braun was supported in part by the German National Fellowship Foundation and J. R. Abney by NIH training grant GM07379.

Received for publication 17 December 1986 and in final form 5 May 1987.

REFERENCES

Abney J. R., J. Braun, and J. C. Owicki. 1987. Lateral interactions among membrane proteins: implications for the organization of gap junctions. *Biophys. J.* 52:441–454.

Abney, J. R., and J. C. Owicki. 1985. Theories of protein-lipid and protein-protein interactions in membranes. *In* Progress in Protein-Lipid Interactions. A. Watts and J. J. H. H. M. de Pont, editors. Elsevier Science Publishers, Amsterdam, the Netherlands. 1–59.

Almers, W., and C. Stirling. 1984. Distribution of transport proteins over animal cell membranes. *J. Membr. Biol.* 77:169–186.

Bald, W. B. 1985. The relative merits of various cooling methods. *J. Microsc.* 140:17–40.

Bevington, P. R. 1969. Data Reduction and Error Analysis for the Physical Sciences. McGraw-Hill Book Co., New York.

Braun, J., J. R. Abney, and J. C. Owicki. 1984. How a gap junction maintains its structure. *Nature (Lond.).* 310:316–318.

Brown, M. S., R. G. W. Anderson, and J. L. Goldstein. 1983. Recycling receptors: the round-trip itinerary of migrant membrane proteins. *Cell.* 32:663–667.

Chandler, D., J. D. Weeks, and H. C. Andersen. 1983. Van der Waals picture of liquids, solids, and phase transformations. *Science (Wash. DC).* 220:787–794.

Escaig, J. 1982. New instruments which facilitate rapid freezing at 83 K and 6 K. *J. Microscopy.* 126:221–229.

Fraser, S. E., and M.-m. Poo. 1982. Development, maintenance, and modulation of patterned membrane topography: models based on the acetylcholine receptor. *Curr. Top. Dev. Biol.* 17:77–100.

Gumbiner, B., and D. Louvard. 1985. Localized barriers in the plasma membrane: a common way to form domains. *Trends Biochem. Sci.* 10:435–438.

Heuser, J. E., T. S. Reese, M. J. Dennis, Y. Jan, L. Jan, and L. Evans. 1979. Synaptic vesicle exocytosis captured by quick freezing and correlated with quantal transmitter release. *J. Cell Biol.* 81:275–300.

Hill, T. L. 1956. Statistical Mechanics. McGraw-Hill Book Co., New York.

Hill, T. L. 1960. Introduction to Statistical Thermodynamics. Addison-Wesley Publishing Co. Inc., Reading, MA.

Holmes, R. P., T. L. Smith, and F. A. Kummerow. 1984. Microheterogeneity in biological membranes. *In* Membrane Processes. Gh. Benga, H. Baum, and F. A. Kummerow, editors. Springer-Verlag, Berlin.

Jain, M. K. 1983. Nonrandom lateral organization in bilayers and biomembranes. *In* Membrane Fluidity in Biology. Vol. 1. R. C. Aloia, editor. Academic Press, Inc., New York. 1–37.

Kopstad, G., and A. Elgsaeter. 1982. Theoretical analysis of specimen cooling rate during impact freezing and liquid-jet freezing of freeze-etch specimens. *Biophys. J.* 40:163–170.

Lado, F. 1967. Pressure-consistent integral equation for classical fluids: hard-sphere solutions. *J. Chem. Phys.* 47:4828–4833.

Levesque, D., J. J. Weis, and L. Reatto. 1985. Pair interaction from structural data for dense classical liquids. *Phys. Rev. Lett.* 54:451–454.

Loewenstein, W. R. 1981. Junctional intercellular communication: the cell-to-cell membrane channel. *Physiol. Rev.* 61:829–913.

Malhotra, S. K. 1983. The Plasma Membrane. John Wiley & Sons, Inc., New York. Chapter 5.

Markovics, J., L. Glass, and G. G. Maul. 1974. Core patterns on nuclear membranes. *Exp. Cell Res.* 85:443–451.

McCloskey, M., and M.-m. Poo. 1984. Protein diffusion in cell membranes: some biological implications. *Int. Rev. Cytol.* 87:19–81.

McQuarrie, D. A. 1976. Statistical Mechanics. Harper & Row Publishers Inc., New York.

Metropolis, N., A. Rosenbluth, M. Rosenbluth, A. Teller, and E. Teller. 1953. Equations of state calculations by fast computing machines. *J. Chem. Phys.* 27:720–733.

Metzger, H., and T. Ishizaka. 1982. Transmembrane signaling by receptor aggregation: the mast cell receptor for IgE as a case study. *Fed. Proc.* 41:7.

Middlehurst, J., and N. S. Parker. 1986. Pair density distribution function of membrane particles at low density. *Biophys. J.* 50:1021–1023.

Oliver, J. M., and R. D. Berlin. 1982. Mechanisms that regulate the structural and functional architecture of cell surfaces. *Int. Rev. Cytol.* 74:55–94.

Pearson, L. T., S. I. Chan, B. A. Lewis, and D. M. Engelman. 1983. Pair distribution functions of bacteriorhodopsin and rhodopsin in model bilayers. *Biophys. J.* 43:167–174.

Pearson, L. T., J. Edelman, and S. I. Chan. 1984. Statistical mechanics of lipid membranes: protein correlation functions and lipid ordering. *Biophys. J.* 45:863–871.

Pearson, R. P., S. W. Hui, and T. P. Stewart. 1979. Correlative statistical analysis and computer modeling of intramembranous particle distributions in human erythrocyte membranes. *Biochim. Biophys. Acta.* 557:265–282.

Peracchia, C. 1985. Cell coupling. *In* The Enzymes of Biological Membranes. Vol. 1. A. Martonosi, editor. Plenum Publishing Corp., New York. 81–160.

Savitzky, A., and M. J. E. Golay. 1964. Smoothing and differention of data by simplified least squares procedures. *Anal. Chem.* 36:1627–1639.

Singer, S. J., and G. L. Nicolson. 1972. The fluid mosaic model of the structure of cell membranes. *Science (Wash. DC).* 175:720–731.

Stoeckenius, W., R. H. Lozier, and R. A. Bogomolni. 1979. Bacteriorhodopsin and the purple membrane of halobacteria. *Biochim. Biophys. Acta.* 505:215–278.

Waxman, S. G., and J. M. Ritchie. 1985. Organization of ion channels in myelinated nerve fibers. *Science (Wash. DC).* 228:1502–1507.

Widom, B. 1967. Intermolecular forces and the nature of the liquid state. *Science (Wash. DC).* 157:375–382.